

Constraints on Individual Supermassive Black Hole Binaries from Pulsar Timing Array Limits on Continuous Gravitational Waves

Katelin Schutz,^{1*} Chung-Pei Ma,²

¹*Department of Physics, University of California at Berkeley, Berkeley CA 94720*

²*Department of Astronomy, University of California at Berkeley, Berkeley CA 94720*

8 April 2016

ABSTRACT

Pulsar timing arrays (PTAs) are placing increasingly stringent constraints on the strain amplitude of continuous gravitational waves emitted by supermassive black hole binaries on subparsec scales. In this paper, we incorporate independent information about the dynamical masses M_{bh} of supermassive black holes in specific galaxies at known distances and use this additional information to further constrain whether or not those galaxies could host a detectable supermassive black hole binary. We estimate the strain amplitudes from individual binaries as a function of binary mass ratio for two samples of nearby galaxies: (1) those with direct dynamical measurements of M_{bh} in the literature, and (2) the 116 most massive early-type galaxies (and thus likely hosts of the most massive black holes) within 108 Mpc from the MASSIVE Survey. Our exploratory analysis shows that the current PTA upper limits on continuous waves (as a function of angular position in the sky) can already constrain the mass ratios of hypothetical black hole binaries in many galaxies in our samples. The constraints are stronger for galaxies with larger M_{bh} and at smaller distances. For the black holes with $M_{\text{bh}} \gtrsim 5 \times 10^9 M_{\odot}$ at the centers of NGC 1600, NGC 4889, NGC 4486 (M87) and NGC 4649 (M60), any binary companion in orbit within the PTA frequency bands would have to have a mass ratio of a few percent or less.

Key words: black hole physics – gravitational waves

1 INTRODUCTION

Pulsar timing arrays (PTAs) are monitored collections of millisecond pulsars, which are rapidly spinning magnetized neutron stars that emit pulses with an extremely precise tempo. Pulsar timing is sensitive to gravitational waves (GWs), which affect the relative arrival time of pulses as measured by observers. Thus, these pulsars act as exquisite probes of GWs and their underlying sources (Sazhin 1978; Detweiler 1979; Hellings & Downs 1983; Romani 1989; Foster & Backer 1990). Three PTAs are currently in operation: the North American Nanohertz Observatory for Gravitational waves (NANOGrav; Jenet et al. 2009), the Parkes Pulsar Timing Array (PPTA; Manchester et al. 2013a), and the European Pulsar Timing Array (EPTA; Janssen et al. 2008). PTAs are sensitive to GW frequencies roughly between 1–100 nHz, a range that depends on the total observational time and observing cadence.

The strongest anticipated source of gravitational waves

in the PTA frequency band is an as-of-yet undetected population of supermassive black hole (SMBH) binaries (Begelman et al. 1980; Wyithe & Loeb 2003; Jaffe & Backer 2003). Under the standard hierarchical picture of galaxy assembly, these SMBH binaries are predicted to form near the centers of galaxies via dynamical friction after galaxy-galaxy mergers, and are expected to be relatively common in a cosmological sense (Sesana et al. 2004). In spite of the theoretical ubiquity of SMBH binaries, many of their properties are still uncertain, such as their formation history (Volonteri et al. 2003) and their dynamical influences on host galaxies (Kormendy et al. 2009).

One expects the whole population of SMBH binaries to emit GWs that add incoherently, forming a roughly isotropic stochastic background of gravitational waves (Rajagopal & Romani 1995; Phinney 2001; Sesana et al. 2008). Upper limits on the stochastic background are becoming tighter as the timing data and analysis algorithms improve (Arzoumanian et al. 2015a; Lentati et al. 2015; Shannon et al. 2015). In addition to the stochastic background, there may be individual sources that emit sufficiently strong continuous GWs

* kschutz@berkeley.edu

to overpower the background. Such individual sources would require relatively nearby massive black hole binaries to exceed the signal of the GW background (Sesana et al. 2009; Sesana & Vecchio 2010).

Thus far, each of the three PTA teams has published an analysis of the upper limit on GWs from individual binary sources. From a sample of 17 pulsars, the NANOGrav 5-year data (Demorest et al. 2013) placed an all-sky upper limit on the strain amplitude of $h_0 < 3.0 \times 10^{-14}$ (95% confidence level) at 10 nHz (Arzoumanian et al. 2014). PPTA reported an upper limit of $h_0 < 1.7 \times 10^{-14}$ at 10 nHz (Zhu et al. 2014) based on observations of 20 pulsars from their data release DR1 in Manchester et al. (2013b). EPTA used data from 42 pulsars and their Bayesian pipeline (assuming the sources do not evolve on the timescale of observations) gives an upper limit of $h_0 < 1.1 \times 10^{-14}$ at 10 nHz (Babak et al. 2015). These values were marginalized over all lines of sight and can vary by a factor of a few at different parts of the sky. These constraints, including their full dependence on angular position in the sky, can be used to probe binary black hole astrophysics.

In this paper we present an exploratory study of the implications of these constraints (as a function of angular position in the sky) for specific known nearby galaxies that could host a detectable SMBH binary. Information about the total mass and location of possible SMBH binaries provides additional constraining power to PTAs and sharpens the limits on the binary properties. For galaxies with such information, we estimate the necessary PTA sensitivity for constraining the existence of a black hole binary. In particular, we examine two samples of galaxies: (1) galaxies in which the masses of the central black holes have been dynamically measured from luminous tracers such as stars, gas, and masers; (2) galaxies in the MASSIVE Survey (Ma et al. 2014), which are the most massive galaxies within ~ 100 Mpc and whose SMBH masses can be inferred by standard scaling relations with host galaxy properties. Using the measured black hole mass and distance to these sources, we estimate the constraints on the binary mass ratio allowed by current PTA upper limits at the angular positions of our sample galaxies.

The rest of the paper is organized as follows. In Section 2, we discuss the physical parameters that can be constrained assuming a signal model consisting of a SMBH binary with circular orbits evolving purely under energy lost via the emission of gravitational waves. In Section 3 we describe the aforementioned samples of galaxies whose SMBHs will be the focus for the rest of the paper. In Section 4, we explore constraints from PTAs on galaxies in our samples and estimate limits on the mass ratios of many hypothetical SMBH binaries. We discuss the results of this paper and future work in Section 5.

2 CONSTRAINED PHYSICAL PARAMETERS

The amplitude of continuous gravitational waves can be parameterized by a dimensionless strain amplitude, h_0 . The GW signal depends on other physical characteristics of a SMBH binary such as the binary inclination and phase, but PTA constraints are reported in terms of this intrinsic amplitude with the other binary characteristics marginalized over. For a SMBH binary at leading post-Newtonian order

under the assumption of circular orbits and evolution purely by energy loss via gravitational radiation, the strain amplitude is given by

$$h_0 = 2.76 \times 10^{-14} \left(\frac{\mathcal{M}}{10^9 M_\odot} \right)^{5/3} \left(\frac{10 \text{ Mpc}}{d_L} \right) \left(\frac{f}{10^{-8} \text{ Hz}} \right)^{2/3}, \quad (1)$$

where f is the frequency of the emitted gravitational waves, d_L is the luminosity distance to the source, and \mathcal{M} is the chirp mass of a binary system consisting of two black holes of mass m_1 and m_2 , with a total mass $M_{\text{bh}} = m_1 + m_2$ and mass ratio $q \equiv m_2/m_1 \leq 1$:

$$\mathcal{M} \equiv \frac{(m_1 m_2)^{3/5}}{(m_1 + m_2)^{1/5}} = M_{\text{bh}} \frac{q^{3/5}}{(1+q)^{6/5}}. \quad (2)$$

Since $q \leq 1$ by definition, it follows that

$$\mathcal{M} \leq 2^{-6/5} M_{\text{bh}} \approx 0.435 M_{\text{bh}}. \quad (3)$$

Thus, for a given total black hole mass M_{bh} , the chirp mass is at a maximum for an equal-mass binary and decreases monotonically as the binary mass ratio m_2/m_1 decreases. The chirp mass is zero for a single black hole.

Combining Eqs. (1) and (3), we obtain the equal-mass strain amplitude

$$h_{0,\text{eq}} = 6.9 \times 10^{-15} \left(\frac{M_{\text{bh}}}{10^9 M_\odot} \right)^{5/3} \left(\frac{10 \text{ Mpc}}{d_L} \right) \left(\frac{f}{10^{-8} \text{ Hz}} \right)^{2/3}. \quad (4)$$

Since the GW strain amplitude h_0 scales monotonically with the chirp mass, $h_{0,\text{eq}}$ corresponds to the maximum allowed value of h_0 for GWs at frequency f emitted by a SMBH binary with total mass M_{bh} at a distance of d_L . This theoretical maximum on the value of h_0 represents the most optimistic limit that PTAs must achieve before being able to detect continuous GWs from SMBH binaries in specific galaxies.

In the next two sections, we will consider galaxies whose central black holes have a total mass M_{bh} that either have been directly measured or can be inferred statistically from their host galaxy properties by using empirical scaling relations. These dynamical mass measurements constrain the total mass M_{bh} but in general cannot distinguish a single black hole from a binary. Several black holes in our sample have sufficiently large M_{bh} and small d_L that the values of $h_{0,\text{eq}}$ from Eq. (4) exceed the current PTA upper limits on h_0 . For these objects, we can further constrain the allowed mass ratio m_2/m_1 of potential binary black holes using the PTA detection limits within the detectable orbital frequencies. To obtain such constraints, we note that for a given d_L , f , and PTA upper limit on h_0 , Eq. (1) provides an upper limit on the chirp mass, which we refer to as \mathcal{M}_{PTA} . We can then use Eq. (2) to estimate the upper limit on m_2/m_1 :

$$\frac{m_2}{m_1} \leq \frac{1 - \sqrt{1 - 4(\mathcal{M}_{\text{PTA}}/M_{\text{bh}})^{5/3}}}{1 + \sqrt{1 - 4(\mathcal{M}_{\text{PTA}}/M_{\text{bh}})^{5/3}}}. \quad (5)$$

We examine the black hole data and present the results in the next two sections.

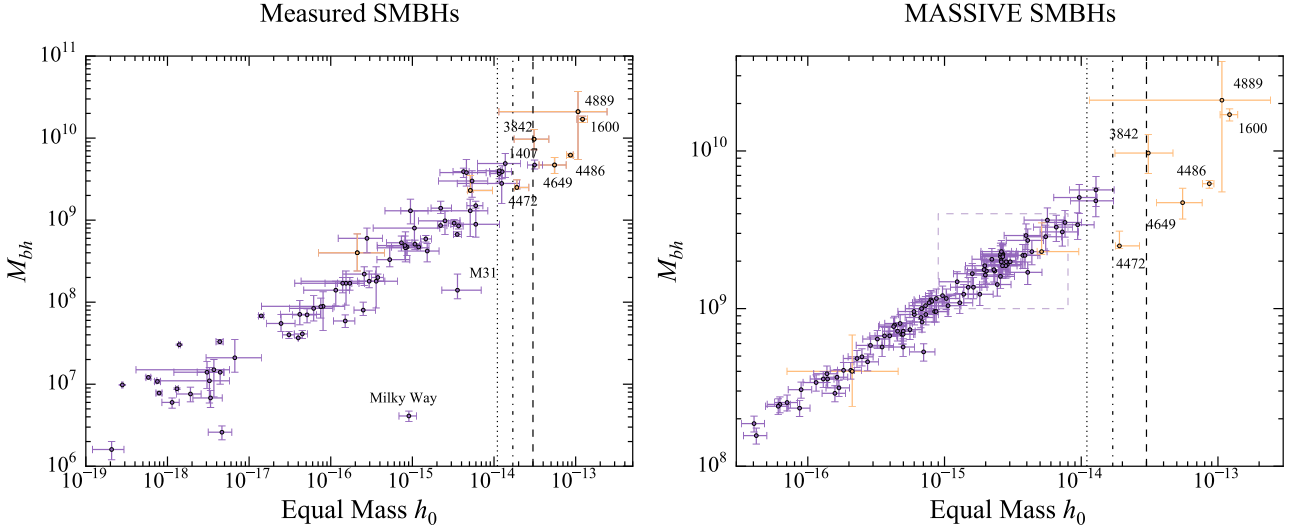


Figure 1. (Left) Black holes with dynamical mass measurements M_{bh} and the strain amplitudes $h_{0,\text{eq}}$ of GWs that would be emitted if the sources were in equal-mass binaries. The vertical lines represent the all-sky upper limits on h_0 from continuous waves by EPTA (dotted), PPTA (dot-dashed), and NANOGrav (dashed). Here h_0 is determined at a GW frequency of 10 nHz. (Right) Same as the left panel but for the sample of 116 most massive early-type galaxies within 108 Mpc targeted by the MASSIVE Survey. The purple points here show black hole masses estimated from the $M_{\text{bh}}-\sigma$ relation, where σ is the measured stellar velocity dispersion of the galaxy (see Section 3.2). The dashed box shows the region spanned by the MASSIVE galaxies when the $M_{\text{bh}}-M_{\text{bulge}}$ relation is instead used to infer M_{bh} . The range of M_{bh} based on M_{bulge} is smaller because the MASSIVE galaxies are selected based on their stellar masses and not velocity dispersions. The eight orange points in both panels represent the galaxies common to both samples, i.e. the MASSIVE galaxies with dynamically measured M_{bh} .

3 TWO SAMPLES OF BLACK HOLES

3.1 Black holes with dynamical mass measurements

We first examine a collection of 77 galaxies whose SMBH masses have been measured directly from kinematics of dynamical tracers within the gravitational sphere of influence of the black holes. These measurements represent over two decades of observational efforts by various collaborations and are obtained from high-angular-resolution spectroscopy of the centers of galaxies within a distance of ~ 120 Mpc from earth. Stars and ionized gas are the most commonly used tracers. Masers and molecular CO gas with organized rotations have been used for a small set of black holes. We take the sample of 72 compiled in [McConnell & Ma \(2013\)](#), and add five measurements published since then: NGC 4526 ([Davis et al. 2013](#); [Gould 2013](#)), M60-UCD1 ([Seth et al. 2014](#)), NGC 1277 ([Walsh et al. 2015a](#)), NGC 1271 ([Walsh et al. 2015b](#)), and NGC 1600 ([Thomas et al. 2016](#)).

These dynamical measurements are sensitive to the total enclosed mass within the angular resolution scale allowed by the instruments and observing conditions at the time the data were taken. With the exception of the center of the Milky Way ([Genzel et al. 2010](#)), the data can not distinguish a single black hole from a binary below this spatial scale. If any one of these galaxies indeed harbors a SMBH binary, their relatively small distances from earth and large masses make them the most promising sites for continuous GW detections by the PTAs. Conversely, an upper limit on GW strain amplitudes from PTAs provides a corresponding upper limit on the allowed binary mass ratio given by Eq. (5).

We depict these data by showing the equal-mass h_0 from Eq. (4) as a function of the measured SMBH mass in the left panel of Figure 1. This value of h_0 corresponds to the largest possible strain for a source with known total M_{bh} and distance. We find a tight relationship as expected, since the scaling with mass is the strongest power law in determining the value of h_0 . The black holes in the Milky Way and M31 are extreme outliers due to their small distances. We show the angular distribution of these possible GW sources relative to the pulsars in various PTAs in the top panel of Figure 2; the angular distribution of sources and pulsars is crucial for detectability because of the PTA antenna pattern. For instance, potential sources which lie along similar lines of sight as the best-timed pulsars will be the most constrained by PTAs.

3.2 The MASSIVE Survey: Most massive black holes within 100 Mpc

The galaxies with dynamical M_{bh} measurements discussed in Sec 3.1 represent a heterogeneous collection of both late-type and early-type galaxies over a wide mass range. The data points shown in the left panel of Figure 1 are therefore a compilation of measurements obtained with differing methods and selection criteria and do not represent results from any well-defined survey or systematic search.

For a more complete census of possible sites for the most massive black holes in the local volume, we consider here the galaxies in the ongoing MASSIVE survey ([Ma et al. 2014](#)). The MASSIVE survey is a volume-limited, multi-wavelength spectroscopic and photometric survey of the 116 most massive early-type galaxies within 108 Mpc in the northern sky

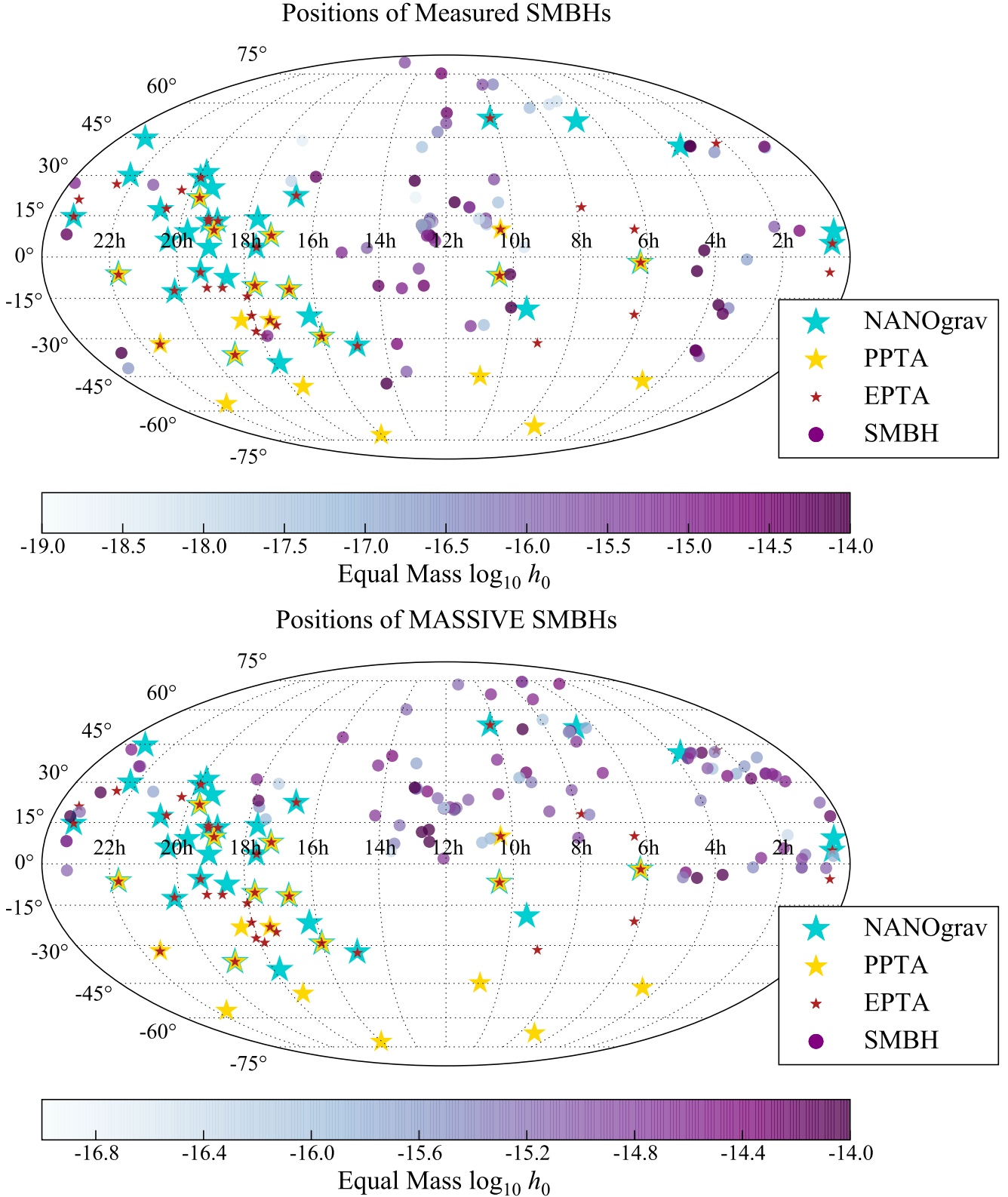


Figure 2. (Top) Angular positions of the supermassive black holes with dynamical mass measurements (purple circles) and the pulsars with timing measurements from NANOGrav (cyan stars), PPTA (yellow stars), and EPTA (red stars). The shading of the purple circles represents the maximum strain amplitudes $h_{0,\text{eq}}$ of GWs (at 10 nHz) given by Eq. (4) that would be emitted if the sources were in equal-mass binaries. (Bottom) Same as the top panel but for the sample of 116 most massive early-type galaxies within 108 Mpc targeted by the MASSIVE Survey. The angular positions of the strongest potential GW sources will influence the comparison between PTAs with different pulsars: due to the steep angular dependence of the PTA antenna function (Corbin & Cornish 2010), the most promising sources to be constrained by future data analysis are dark purple circles that lie along similar lines of sight as the best-timed PTA pulsars.

(above a declination of -6°). The galaxies in the survey are selected based on stellar mass, and the survey is complete to an absolute K -band magnitude of $M_K = -25.3$ mag, corresponding to a stellar mass of $M_* \approx 10^{11.5} M_\odot$. The MASSIVE galaxies reside in diverse environments. Despite their large stellar masses, only 9 of the 116 galaxies reside in the three well-known clusters Virgo, Perseus and Coma. A total of 26 MASSIVE galaxies are relatively isolated and considered “groupless” according to the group catalog of Crook et al. (2007), containing fewer than three group members.

Eight galaxies in the MASSIVE sample have published black hole masses in the literature: NGC 4486 (Gebhardt et al. 2011; Walsh et al. 2013), NGC 4472 and NGC 7619 (Rusli et al. 2013), NGC 4649 (Shen & Gebhardt 2010), NGC 3842 and NGC 4889 (McConnell et al. 2011, 2012), NGC 7052 (van der Marel & van den Bosch 1998), and NGC 1600 (Thomas et al. 2016). These galaxies are located at the high end of the M_{bh} and galaxy bulge mass relation. The ongoing MASSIVE survey is expected to provide at least 15 new measurements of M_{bh} .

To estimate the dynamical value of M_{bh} for the entire MASSIVE sample, we follow the standard practice of using a galaxy’s measured stellar velocity dispersion σ or bulge mass M_{bulge} and converting them into M_{bh} from well-established scaling relations between black hole and galaxy properties. We use σ from Ma et al. (2014, Table 3), and we obtain the bulge mass from M_K in the same table and convert it to M_{bulge} using $\log_{10} M_* = 10.58 - 0.44(M_K + 23)$. We assign the total stellar mass to the bulge since the MASSIVE galaxies are all early-type galaxies and most of them are elliptical galaxies.

In the right panel of Figure 1 we show $h_{0,\text{eq}}$ for equal-mass binaries as a function of M_{bh} inferred for MASSIVE galaxies, using the $M_{\text{bh}}-\sigma$ relation of McConnell & Ma (2013). The range of M_{bh} and hence h_0 is smaller when using the $M_{\text{bh}}-M_{\text{bulge}}$ relation (indicate by the dashed box) because the MASSIVE survey is selected based on galaxy mass and not σ . Even though M_{bulge} and σ of galaxies are positively correlated, there is a large scatter in σ at a given stellar mass. For the rest of the paper, we focus on masses inferred by the $M_{\text{bh}}-\sigma$ relation.

The angular positions of the MASSIVE galaxies and PTA pulsars are plotted in the bottom panel of Figure 2. We note that several MASSIVE galaxies are along almost the same line of sight as several PTA pulsars, enhancing their detectability owing to the steep angular dependence of the PTA antenna patterns (Wahlquist 1987; Corbin & Cornish 2010).

4 CONSTRAINTS ON INDIVIDUAL BINARY MASS RATIOS

As shown in Figure 1, the $h_{0,\text{eq}}$ values for a subset of potential SMBH binaries are above the current all-sky PTA upper limits (vertical lines). In this section we examine these potential sources further, as well as sources that are constrained because they are located in regions of the sky with greater PTA sensitivity, as illustrated in Zhu et al. (2014, Figure 11) and Babak et al. (2015, Figures 7 & 8). As discussed in Section 2, we can use the current PTA limits on

Mass Ratio Upper Limits

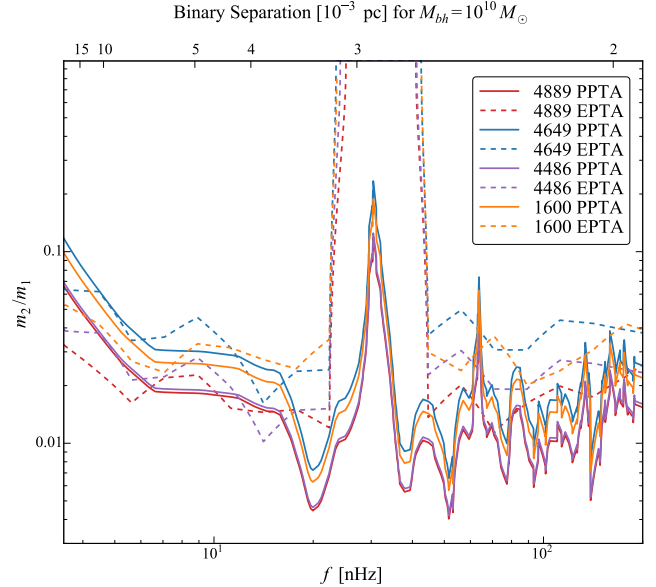


Figure 3. GW frequency dependence of the upper limits on the black hole mass ratio ($m_2 \leq m_1$ by definition) of hypothetical binaries located in the centers of NGC 4889 (red), NGC 4486 (purple), NGC 4649 (blue), and NGC 1600 (orange). For each galaxy, the limit on m_2/m_1 is computed using the 95% upper limits on h_0 from EPTA (dashed curve) and PPTA (solid curve). Also shown is the corresponding binary orbital separation calculated assuming a $10^{10} M_\odot$ SMBH binary. Here we use M_{bh} for NGC 4486 from Gebhardt et al. (2011) and we assume that all SMBH masses are given by their mean measured values.

continuous GWs to obtain an upper limit on the binary mass ratio m_2/m_1 for each source using Eq. (5). For the rest of our analysis, we focus on the limits from EPTA and PPTA, which have the strongest constraints to date. In particular, we use their constraint maps, which include the full angular dependence of these constraints. We note here that by simply using the h_0 constraint maps reported by these two PTAs, we are not able to constrain the binary mass ratio with a high degree of certainty. To do that properly, one would need many signal injections in the PTA data which sample the possible mass ratios and other properties of the SMBH binary. This more rigorous analysis is beyond the scope of this exploratory study. Nevertheless, we report constraints using the methods outlined above, noting that our results serve as a benchmark and as a proof of concept.

We further note that despite the simple frequency scaling in Eqs. (1) and (4), the constraints on h_0 from the full analyses of PTA data have more complicated features in the frequency dependence due to various degeneracies between timing models and GW signals. The frequency dependence of the PTA constraints on continuous GWs is illustrated by Arzoumanian et al. (2014, Figure 6), Zhu et al. (2014, Figure 9), and Babak et al. (2015, Figure 6). All three figures show that the constraints on h_0 are especially weak at frequencies corresponding to 1 and 2 inverse years, since pulsar timing systematics coming from the earth’s orbit are partly degenerate with a GW signal. There is also an upward trend

Table 1. Upper limits on the binary mass ratio, m_2/m_1 , for SMBHs with measured total masses and for SMBHs in MASSIVE galaxies with their total masses inferred by standard scaling relations. We report limits from EPTA and PPTA constraint maps (taking into account the constraint at the angular position of each galaxy) at three representative GW frequencies. The constraints vary between the two PTAs depending on the angular position of the possible source and the frequency. Also listed are the total dynamical mass (measured or inferred), the distance, and the strain amplitude of GWs emitted in the scenario where each SMBH is in an equal-mass binary, which represents the maximum possible strain.

Galaxy	M_{bh}	d_L	$h_{0,\text{eq}}$	$(m_2/m_1)_{\text{max}}$ (EPTA)			$(m_2/m_1)_{\text{max}}$ (PPTA)		
Measured	$[10^9 M_\odot]$	[Mpc]	$[10^{-14}]$	6 nHz	10 nHz	100 nHz	6 nHz	10 nHz	100 nHz
NGC 1600	17	63.8	12	0.026	0.032	0.022	0.030	0.026	0.011
NGC 4889	21	102	11	0.020	0.019	0.018	0.021	0.018	0.008
NGC 4486	6.2	16.7	8.6	0.023	0.024	0.023	0.022	0.018	0.008
NGC 4486 ¹	3.3	16.7	3.0	0.071	0.074	0.071	0.069	0.058	0.026
NGC 4649	4.7	16.5	5.5	0.037	0.038	0.038	0.035	0.030	0.013
NGC 1407	4.7	29.0	3.1	0.11	0.12	0.072	0.12	0.10	0.038
NGC 3842	9.7	98.4	3.1	0.084	0.083	0.12	0.091	0.077	0.030
NGC 4472	2.4	16.7	1.8	0.13	0.13	0.13	0.13	0.10	0.040
NGC 1277	4.9	71.0	1.4	0.42	0.74	-	-	-	0.25
NGC 1550	3.8	53.0	1.2	-	-	0.49	-	-	0.15
IC 1459	2.8	30.9	1.2	0.20	0.26	0.14	0.21	0.17	0.061
NGC 3091	3.7	52.7	1.1	0.45	0.55	-	0.30	0.23	0.077
NGC 5516	3.5	60.1	0.92	0.24	0.41	0.21	0.15	0.13	0.047
NGC 3115	0.89	9.5	0.60	-	-	-	-	-	0.20
NGC 1332	1.5	22.7	0.60	-	-	-	-	-	0.31
NGC 1399	1.3	20.9	0.51	-	-	-	-	-	0.30
NGC 7619	2.3	53.9	0.51	-	-	-	-	-	0.35
NGC 6086	3.8	139	0.46	-	-	0.68	-	-	0.19
A1836-BCG	3.9	158	0.42	-	-	-	-	-	0.17
NGC 4594	0.67	10.0	0.35	-	-	-	-	-	0.28
NGC 4374	0.92	18.5	0.32	-	-	-	-	-	0.51
A3565-BCG	1.4	54.4	0.22	-	-	-	-	-	0.49
MASSIVE	$[10^9 M_\odot]$	[Mpc]	$[10^{-14}]$	6 nHz	10 nHz	100 nHz	6 nHz	10 nHz	100 nHz
NGC 7681	5.6	96.8	1.3	0.20	0.25	0.12	0.55	0.37	0.10
NGC 2693	4.8	74.4	1.3	0.56	0.38	0.42	-	-	0.18
NGC 7436	5.1	106.6	0.97	0.32	0.43	0.17	-	-	0.15
NGC 1453	3.4	56.4	0.94	-	-	-	-	-	0.20
NGC 7619	3.2	54	0.88	0.34	-	0.30	-	-	0.15
NGC 6482	3.1	61.4	0.73	0.23	0.31	0.16	0.43	0.31	0.09
NGC 0057	3.3	76.3	0.67	-	-	-	-	-	0.38
NGC 2832	3.6	105	0.57	-	-	-	-	-	0.80
NGC 5353	1.7	41.1	0.41	-	-	-	-	-	0.40
NGC 4555	2.9	104	0.39	-	-	-	-	-	0.35
NGC 6575	2.3	106	0.26	-	-	-	-	-	0.83

at lower frequencies ($f \lesssim 10$ nHz) due to the quadratic spin-down model fit. As shown in [Zhu et al. \(2014, Figure 10\)](#), the spectral shape of PPTA constraints on h_0 are almost exactly the same as a function of line-of-sight direction modulo an overall vertical shift depending on the PTA sensitivity as a function of angular position. Meanwhile, the frequency dependence of EPTA constraints have a weak directional dependence.

Figure 3 shows our resulting upper limits on the SMBH binary mass ratio as a function of GW frequency for NGC 1600 (orange curves), NGC 4889 (red curves), NGC 4486 (M87; purple curves), and NGC 4649 (M60; blue curves). Depending on the exact frequency, we obtain a tighter constraint on the mass ratio from either EPTA (dashed curves) or PPTA (solid curves). We emphasize that we are assuming that the SMBH masses are given by their mean measured value. We anticipate that marginalizing over uncertainties on the SMBH mass (based on observational measurements)

using a full analysis of the PTA data could change the constraints. This is particularly true for NGC 4889, whose mass measurement has the largest observational uncertainties. We again note that the full analysis of PTA data is beyond the scope of this exploratory study.

In Table 1 we tabulate the upper limits on the binary black hole mass ratios at three separate GW frequencies (6 nHz, 10 nHz and 100 nHz) for the sources in our two samples of galaxies that can be constrained by the current PPTA and EPTA limits. We chose these as representative GW frequencies which have relatively little degeneracy between a GW signal and the pulsar timing model. We also include the total dynamical mass of the black hole and the distance to each galaxy. The top galaxies have dynamically measured

¹ We include the lower M_{bh} for M87 from [Walsh et al. \(2013\)](#) based on gas rather than stellar kinematics. We adjust this measurement to be consistent with a measured distance of 16.7 Mpc.

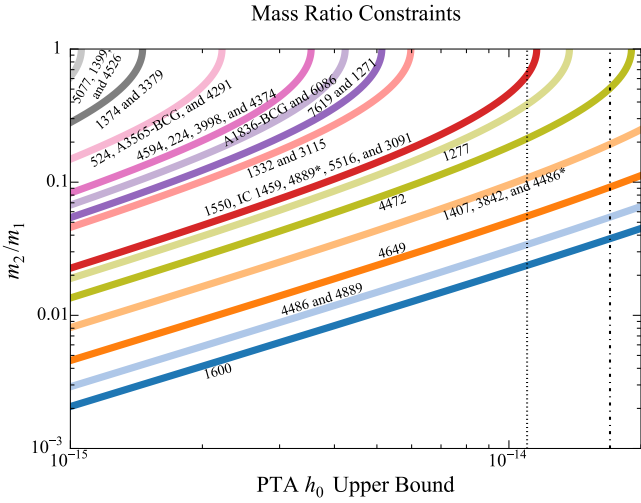


Figure 4. Upper limits on the black hole mass ratio ($m_2 \leq m_1$ by definition) of hypothetical binaries located in various galaxies as a function of the PTA limit on h_0 at the angular position of each galaxy, assuming a GW frequency of 10 nHz. The two vertical lines indicate the all-sky 95% upper limits on h_0 from EPTA (dotted; Babak et al. 2015) and PPTA (dot-dashed; Zhu et al. 2014) at the same frequency. As the limits on continuous GWs from PTAs become more stringent, the allowed binary mass ratios become smaller, and the constraints are applicable to more galaxies. For two galaxies, we have included two curves for each: NGC 4486 (upper curve denoted by an asterisk for M_{bh} from Walsh et al. 2013; lower curve for M_{bh} from Gebhardt et al. 2011), and NGC 4889 (upper curve denoted by an asterisk for the very conservative 1σ lower bound on M_{bh} from McConnell et al. 2011; lower curve for their median M_{bh}).

black hole masses; several additional MASSIVE galaxies do not have published dynamical measurements yet and the total black hole mass is inferred from the $M_{\text{bh}}-\sigma$ relation. As shown by Table 1 and Figure 3, we are able to constrain the mass ratio to be less than a few percent for potential binary black holes on circular orbits (within the PTA frequency window) in several galaxies based on the constraint on h_0 at their positions in the sky. In spite of the fact that our results are obtained under simplifying assumptions already mentioned, we have demonstrated as a proof of concept that one can achieve percent-level constraints on SMBH binaries using existing PTA data.

Upcoming continuous GW analyses of the NANOGrav 9-year data (Arzoumanian et al. 2015b) and the PPTA DR2 data (Shannon et al. 2015) will likely place stronger limits on h_0 than those compiled in this paper. In anticipation of these tighter limits, we illustrate in Figure 4 the dependence of the maximum binary mass ratio as a function of the upper limit on h_0 for galaxies with measured SMBH masses. This figure illustrates future science that can be done to constrain nearby, massive SMBH binaries by combining upcoming PTA data with dynamical measurements of specific black holes. Based on Figure 4, we project that constraints on the black holes with known masses in ~ 30 galaxies can be obtained when the PTA sensitivity to continuous GWs from individual sources is lowered to $h_0 \approx 10^{-15}$ at the directions in the sky where these galaxies are located.

Meanwhile, the galaxies that are below the current and

upcoming detection thresholds are potential GW “hot spots” for ongoing and future PTA searches for continuous GWs (a topic which has been previously explored in, for instance, Simon et al. 2014 and Burt et al. 2011). The analysis of these particular hotspots and their implications for upcoming PTAs will be the subject of future work.

5 DISCUSSION

We have demonstrated, as a proof of concept, the efficacy of using PTA limits on GW strain amplitudes to place constraints on individual prospective SMBH binaries in our local volume by leveraging information about their total dynamical masses and distances. In particular, we have examined two samples of galaxies and placed upper limits on the mass ratio of SMBH binaries with sub-parsec orbital separations in a number of galaxies. To achieve this, we have used the latest and most stringent upper limits on h_0 (as a function of direction in the sky) from PPTA and EPTA.

For several SMBHs with $M_{\text{bh}} \gtrsim 5 \times 10^9 M_{\odot}$, e.g., NGC 4889, NGC 4486, NGC 4649, and NGC 1600, we find that the mass ratio of a hypothetical binary would have to be less than around a few percent, or even as low as a few tenths of a percent in some PTA frequency bands (see Figs. 3 and 4 and Table 1). It is interesting to note that these limits on SMBH binary mass ratios in massive galaxies are similar to the limit for the SMBH in the Milky Way obtained from individual stellar motions. The exquisite dynamical measurements of the Galactic Center constrain a second black hole to be less than $\sim 10^5 M_{\odot}$, i.e., a binary mass ratio of $\lesssim 2.5\%$ (Genzel et al. 2010). PTAs are currently not competitive as a constraint on the SMBH at the Galactic Center due to its low M_{bh} (see Fig. 1) and the steep mass dependence in Eqs. (1) and (4). As we have shown, however, PTAs are a powerful tool for providing percent-level limits on the most massive SMBH binary ratios out to ~ 100 Mpc.

Although the emission of GWs tends to circularize binary orbits, interactions of a SMBH binary with the surrounding stars and gas before it enters the GW-driven phase can make the orbits more elliptical over time, especially for binaries with unequal masses (Peters & Mathews 1963; Sesana 2013, 2010; Sesana et al. 2006, 2004, 2009; Roedig et al. 2011; Merritt et al. 2007; Matsubayashi et al. 2007; Quinlan 1996; Preto et al. 2011; Armitage & Natarajan 2005; Cuadra et al. 2009). At the characteristic eccentricities quoted by these studies, the detection power of PTAs at low frequencies (where GW-induced timing residuals are expected to be largest) is greatly suppressed (Enoki & Nagashima 2007; Sesana et al. 2004; Kocsis & Sesana 2011). Therefore, even if there is a very unequal-mass SMBH binary in NGC 1600, NGC 4889, NGC 4486, or NGC 4649, its orbit will likely be highly eccentric and render a detection improbable in the near future. Upcoming analyses based on the formalism developed in Taylor et al. (2016) could shed light on this issue further.

Based on the benchmarks that we have set here, we anticipate that a full analysis of existing or upcoming PTA data will prove extremely useful by providing more accurate constraints on the SMBH binaries in our sample galaxies. By searching the full parameter space of binary mass ratios, binary inclination angles, etc., such analysis would provide

meaningful limits on the astrophysics of SMBH binaries and their relationship with the host galaxies. We further anticipate that such analysis would be useful to incorporate into searches for anisotropy in the gravitational wave background (such as the one performed in Taylor et al. 2015). New dynamical measurements of M_{bh} from the MASSIVE Survey will also remove the uncertainties associated with using the $M_{\text{bh}}-\sigma$ relation as a mass proxy and provide more realistic constraints for potential binaries in those galaxies.

ACKNOWLEDGEMENTS

It is an immense pleasure to thank Justin Ellis, Matthew Kerr, Adrian Liu, Nicholas McConnell, Scott Ransom, Leo Stein, and Xingjiang Zhu for useful conversations and correspondence pertaining to this work. We also wish to thank Stanislav Babak and Xingjiang Zhu (on behalf of EPTA and PPTA, respectively) for providing us with their constraint maps. Finally, we thank our referee, Alberto Sesana, for his detailed comments on the original version of the manuscript. KS is supported by a Hertz Foundation Fellowship and by a National Science Foundation Graduate Research Fellowship. CPM is supported in part by National Science Foundation grant AST-1411945.

REFERENCES

- Armitage P. J., Natarajan P., 2005, *ApJ*, **634**, 921
 Arzoumanian Z., et al., 2014, *ApJ*, **794**, 141
 Arzoumanian Z., et al., 2015a, preprint, ([arXiv:1508.03024](https://arxiv.org/abs/1508.03024))
 Arzoumanian Z., et al., 2015b, preprint, ([arXiv:1505.07540](https://arxiv.org/abs/1505.07540))
 Babak S., et al., 2015, preprint, ([arXiv:1509.02165](https://arxiv.org/abs/1509.02165))
 Begelman M. C., Blandford R. D., Rees M. J., 1980, *Nature*, **287**, 307
 Burt B. J., Lommen A. N., Finn L. S., 2011, *ApJ*, **730**, 17
 Corbin V., Cornish N. J., 2010, preprint, ([arXiv:1008.1782](https://arxiv.org/abs/1008.1782))
 Crook A. C., Huchra J. P., Martimbeau N., Masters K. L., Jarrett T., Macri L. M., 2007, *ApJ*, **655**, 790
 Cuadra J., Armitage P. J., Alexander R. D., Begelman M. C., 2009, *MNRAS*, **393**, 1423
 Davis T. A., Bureau M., Cappellari M., Sarzi M., Blitz L., 2013, *Nature*, **494**, 328
 Demorest P. B., et al., 2013, *ApJ*, **762**, 94
 Detweiler S., 1979, *ApJ*, **234**, 1100
 Enoki M., Nagashima M., 2007, *Progress of Theoretical Physics*, **117**, 241
 Foster R. S., Backer D. C., 1990, *ApJ*, **361**, 300
 Gebhardt K., Adams J., Richstone D., Lauer T. R., Faber S. M., Gültekin K., Murphy J., Tremaine S., 2011, *ApJ*, **729**, 119
 Genzel R., Eisenhauer F., Gillessen S., 2010, *Reviews of Modern Physics*, **82**, 3121
 Gould A., 2013, preprint, ([arXiv:1303.0834](https://arxiv.org/abs/1303.0834))
 Hellings R. W., Downs G. S., 1983, *ApJ*, **265**, L39
 Jaffe A. H., Backer D. C., 2003, *ApJ*, **583**, 616
 Janssen G. H., Stappers B. W., Kramer M., Purver M., Jessner A., Cognard I., 2008, in Bassa C., Wang Z., Cumming A., Kaspi V. M., eds, American Institute of Physics Conference Series Vol. 983, 40 Years of Pulsars: Millisecond Pulsars, Magnetars and More. pp 633–635, [doi:10.1063/1.2900317](https://doi.org/10.1063/1.2900317)
 Jenet F., et al., 2009, preprint, ([arXiv:0909.1058](https://arxiv.org/abs/0909.1058))
 Kocsis B., Sesana A., 2011, *MNRAS*, **411**, 1467
 Kormendy J., Fisher D. B., Cornell M. E., Bender R., 2009, *ApJS*, **182**, 216
 Lentati L., et al., 2015, *MNRAS*, **453**, 2576
 Ma C.-P., Greene J. E., McConnell N., Janish R., Blakeslee J. P., Thomas J., Murphy J. D., 2014, *ApJ*, **795**, 158
 Manchester R. N., et al., 2013a, *Publ. Astron. Soc. Australia*, **30**, 17
 Manchester R. N., et al., 2013b, *Publ. Astron. Soc. Australia*, **30**, 17
 Matsubayashi T., Makino J., Ebisuzaki T., 2007, *ApJ*, **656**, 879
 McConnell N. J., Ma C.-P., 2013, *ApJ*, **764**, 184
 McConnell N. J., Ma C.-P., Gebhardt K., Wright S. A., Murphy J. D., Lauer T. R., Graham J. R., Richstone D. O., 2011, *Nature*, **480**, 215
 McConnell N. J., Ma C.-P., Murphy J. D., Gebhardt K., Lauer T. R., Graham J. R., Wright S. A., Richstone D. O., 2012, *ApJ*, **756**, 179
 Merritt D., Mikkola S., Szell A., 2007, *ApJ*, **671**, 53
 Peters P. C., Mathews J., 1963, *Physical Review*, **131**, 435
 Phinney E. S., 2001, ArXiv Astrophysics e-prints,
 Preto M., Berentzen I., Berczik P., Spurzem R., 2011, *ApJ*, **732**, L26
 Quinlan G. D., 1996, *New Astron.*, **1**, 35
 Rajagopal M., Romani R. W., 1995, *ApJ*, **446**, 543
 Roedig C., Dotti M., Sesana A., Cuadra J., Colpi M., 2011, *MNRAS*, **415**, 3033
 Romani R. W., 1989, in Ögelman H., van den Heuvel E. P. J., eds, NATO Advanced Science Institutes (ASI) Series C Vol. 262, NATO Advanced Science Institutes (ASI) Series C. p. 113
 Rusli S. P., et al., 2013, *AJ*, **146**, 45
 Sazhin M. V., 1978, *Soviet Ast.*, **22**, 36
 Sesana A., 2010, *ApJ*, **719**, 851
 Sesana A., 2013, *Classical and Quantum Gravity*, **30**, 224014
 Sesana A., Vecchio A., 2010, *Classical and Quantum Gravity*, **27**, 084016
 Sesana A., Haardt F., Madau P., Volonteri M., 2004, *ApJ*, **611**, 623
 Sesana A., Haardt F., Madau P., 2006, *ApJ*, **651**, 392
 Sesana A., Vecchio A., Colacino C. N., 2008, *MNRAS*, **390**, 192
 Sesana A., Vecchio A., Volonteri M., 2009, *MNRAS*, **394**, 2255
 Seth A. C., et al., 2014, *Nature*, **513**, 398
 Shannon R. M., et al., 2015, preprint, ([arXiv:1509.07320](https://arxiv.org/abs/1509.07320))
 Shen J., Gebhardt K., 2010, *ApJ*, **711**, 484
 Simon J., Polin A., Lommen A., Stappers B., Finn L. S., Jenet F. A., Christy B., 2014, *ApJ*, **784**, 60
 Taylor S. R., et al., 2015, *Physical Review Letters*, **115**, 041101
 Taylor S. R., Huerta E. A., Gair J. R., McWilliams S. T., 2016, *ApJ*, **817**, 70
 Thomas J., Ma C.-P., McConnell N., Greene J., Blakeslee J., Janish R., 2016, *Nature*, in press
 Volonteri M., Haardt F., Madau P., 2003, *ApJ*, **582**, 559
 Wahlquist H., 1987, *General Relativity and Gravitation*, **19**, 1101
 Walsh J. L., Barth A. J., Ho L. C., Sarzi M., 2013, *ApJ*, **770**, 86
 Walsh J. L., van den Bosch R. C. E., Gebhardt K., Yıldırım A., Richstone D. O., Gültekin K., Husemann B., 2015a, preprint, ([arXiv:1511.04455](https://arxiv.org/abs/1511.04455))
 Walsh J. L., van den Bosch R. C. E., Gebhardt K., Yıldırım A., Gültekin K., Husemann B., Richstone D. O., 2015b, *ApJ*, **808**, 183
 Wyithe J. S. B., Loeb A., 2003, *ApJ*, **595**, 614
 Zhu X.-J., et al., 2014, *MNRAS*, **444**, 3709
 van der Marel R. P., van den Bosch F. C., 1998, *AJ*, **116**, 2220